Title

Developing Personalized Models for Predicting Neurodegeneration Using Plasma Neurofilament Light Chain in Alzheimer's Disease: Preliminary Findings from the ADNI Cohort

ISBN

9798190915211

Author

Liu, Shutong

Publication Date

2026-09-09

Peer reviewed|Thesis/dissertation

Developing Personalized Models for Predicting Neurodegeneration Using Plasma Neurofilament Light Chain in Alzheimer's Disease: Preliminary Findings from the ADNI Cohort

by

Shutong Liu

THESIS

Submitted in partial satisfaction of the requirements for degree of

MASTER OF SCIENCE

in

Biomedical Imaging

in the

GRADUATE DIVISION

of the

UNIVERSITY OF CALIFORNIA, SAN FRANCISCO

Approved:

DocuSigned by:
Duygu Tosun-Turgut
A2C3822F2671486...

Duygu Tosun-Turgut

Chair

DocuSigned by:
Janine Lupo
[illegible]

Janine Lupo

DocuSigned by:
Andreas Rauschecker
[illegible]

Andreas Rauschecker

DocuSigned by:
Srikantan Nagarajan
4C21BC1B9EB145E...

Srikantan Nagarajan

Committee Members

Acknowledgments

In what now feels like the blink of an eye, this thesis has grown from an initially uncertain research proposal into the complete and coherent work presented here. Looking back on this process, I know that my own efforts alone would never have brought me to this point. I am deeply grateful to everyone who offered their guidance, encouragement, and support along the way.

First and foremost, I would like to express my sincere gratitude to my thesis mentor, Professor Duygu Tosun-Turgut. I am grateful to her for giving me the opportunity to study Alzheimer's disease and for guiding me throughout this project. Through this experience, I gained a deeper understanding of the field and learned to apply a range of statistical methods to complex research questions. Her patience, expertise, and thoughtful guidance shaped every stage of this work, from the development of the research direction to the analysis and writing. This project would not have been possible without her mentorship.

I would also like to sincerely thank Pamela Thropp, Isabella Hausle, and Alison Myoraku for their invaluable academic support throughout this project. Pamela generously helped me refine and polish my writing, while Alison provided important methodological guidance that strengthened my approach to the research questions. Ellie also made significant contributions to the data analysis and model development, offering expertise that was essential to the progress of this work. I am deeply grateful for their time, patience, and thoughtful assistance.

I am deeply grateful to my family and friends for their constant understanding and support. Whenever I felt overwhelmed by the data, analyses, or writing, they were always there to listen, comfort me, and remind me to keep going. Their encouragement became an important source of strength throughout this journey.

I would also like to thank all the professors, faculty members, and instructors of the UCSF Master of Science in Biomedical Imaging program. The breadth, depth, and forward-looking nature of the program introduced me to many areas of biomedical imaging and

helped me develop a deeper understanding of both imaging science and scientific research. This experience has expanded my knowledge, strengthened my skills, and helped clarify the direction I hope to pursue in the future.

Finally, I would like to acknowledge myself—for continuing through uncertainty, setbacks, and many moments of starting over. I am grateful that I chose to persevere and gradually transformed an uncertain initial idea into the thesis it is today. This journey was not always easy, but it allowed me to recognize my own growth and gave me greater confidence as I move toward the next chapter.

Developing Personalized Models for Predicting Neurodegeneration Using Plasma Neurofilament Light Chain in Alzheimer's Disease: Preliminary Findings from the ADNI Cohort

Shutong Liu

Abstract

Plasma neurofilament light chain (NfL) is a sensitive blood-based biomarker of neuroaxonal injury with potential value for predicting Alzheimer's disease (AD)-related neurodegeneration. However, plasma NfL is influenced by physiological factors, including age, body mass index (BMI), and renal function. Besides, it remains unclear whether adjusted NfL measurements can predict subsequent structural brain changes during the preclinical stage of AD. Using data from the Alzheimer's Disease Neuroimaging Initiative (ADNI), this study developed individualized plasma NfL reference distributions and evaluated their ability to predict longitudinal MRI-measured neurodegeneration. Generalized Additive Models for Location, Scale, and Shape were fitted in CU Aβ− reference participants with valid eGFR data (n=378) to derive age-, BMI-, and eGFR-adjusted NfL Z-scores. Linear mixed-effects models were then used to test whether baseline and longitudinal NfL Z-scores were associated with changes in hippocampal volume, AD-signature cortical thickness, and lateral ventricular volume among Aβ+ participants. Expected plasma NfL increased with age and lower eGFR and decreased with higher BMI. Adjusted NfL Z-scores increased progressively across the AD continuum. However, baseline NfL Z-score did not significantly predict longitudinal change in any MRI outcome in the CU Aβ+, cognitively impaired Aβ+, or Early AD Continuum cohorts. In an exploratory subset, a greater annualized increase in NfL Z-score was associated with faster hippocampal volume decline (β = −0.225, P = 0.045), although the association did not remain significant after multiple-comparison correction. These findings support physiological adjustment for individualized interpretation of plasma NfL. Although a single baseline measurement did not predict subsequent MRI change, longitudinal NfL dynamics may provide a more informative signal of ongoing

neurodegeneration and warrant further evaluation in larger cohorts with more frequent repeated measurements.

Table of Contents

List of Figures

List of Tables

List of Abbreviations

Aβ Amyloid beta

Aβ42/40 Amyloid beta 42-to-40 ratio

AD Alzheimer's disease

ADNI Alzheimer's Disease Neuroimaging Initiative

APOE Apolipoprotein E

BCT Box-Cox *t* distribution

BMI Body mass index

CI Cognitively impaired

ComBat-GAM ComBat generalized additive model

CSF Cerebrospinal fluid

CU Cognitively unimpaired

eGFR Estimated glomerular filtration rate

FDR False discovery rate

GAM Generalized additive model

GAMLSS Generalized additive models for location, scale, and shape

ICV Intracranial volume

LME Linear mixed-effects model

MCI Mild cognitive impairment

MRI Magnetic resonance imaging

NfL Neurofilament light chain

PET Positron emission tomography

p-tau Phosphorylated tau

ROI Region of interest

SD Standard deviation

Introduction

Alzheimer's disease (AD) is a progressive neurodegenerative disorder affecting over 55 million people worldwide.[1] AD pathology is defined by the accumulation of beta-amyloid (Aβ) plaques followed by tau neurofibrillary tangles, then synaptic dysfunction and atrophy (e.g. hippocampal atrophy and cortical thinning) and ultimately cognitive impairment and decline.[1] Evidence suggests that AD pathology develops long before symptom onset and clinical diagnosis. In a disease-progression model anchored to the time of AD diagnosis, AD biomarkers were estimated to emerge years before clinical symptom onset: CSF amyloid (Aβ42) 18 years before, phosphorylated tau, p-tau181 (11 years), neurofilament light chain, NfL (9.5 years), hippocampal volume changes (8 years), and cognitive decline (6 years).[2,3] While these events follow a stereotypical order, preclinical individuals who are amyloid-positive (i.e., show evidence of AD pathology but remain cognitively unimpaired [CU]) exhibit substantial heterogeneity in their timing for symptom onset. Indeed, some may never develop cognitive impairment. A critical milestone to proactively monitor in these preclinical individuals is accelerated neurodegeneration, or atrophy, to assess their risk for clinical symptom onset. The fact that markers of neurodegeneration become abnormal several years before diagnosis underscores their potential value for identifying individuals at risk during the preclinical stages of the disease, a period that is increasingly targeted by emerging disease-modifying therapies.

Structural MRI is currently used to quantify neurodegeneration using established measurements such as hippocampal atrophy, cortical thinning, and ventricular enlargement.[5,6] However, MRI is costly, time-consuming, and lacks the scalability required for routine clinical practice. These constraints have driven recent interest in fluid biomarkers, particularly blood-based biomarkers, which are inexpensive, widely available, minimally invasive, and scalable but more importantly have shown immense promise in the AD domain.

Plasma neurofilament light chain (NfL) has emerged as a sensitive marker of axonal injury. NfL is a cytoskeletal protein released into blood following neuronal damage[7,8] and can be accurately quantified at picogram-per-milliliter concentrations.[9] Although it is a non-specific marker of neuronal damage, plasma NfL is elevated throughout the AD continuum and is associated with MRI-measured neurodegeneration measures, accelerated brain atrophy, progression from mild cognitive impairment (MCI) to AD dementia, and cognitive decline.[10,11,12] Importantly, elevated NfL levels precede detectable hippocampal volume loss by approximately 1.5 years,[2] suggesting that plasma NfL may reflect early neuronal injury before structural MRI changes become visible. This supports its potential role as an early screening biomarker for downstream accelerated neurodegeneration.

Before plasma NfL can be reliably utilized to forecast neurodegeneration, it is essential to deeply understand its expected normal biological variability. Because blood-based biomarkers circulate systemically, their concentrations are strongly modulated by physiological and demographic factors independent of central nervous system pathology. Normal aging involves a physiological increase in NfL, reflecting cumulative subclinical neuronal turnover and age-related changes in cerebrospinal fluid clearance dynamics.[20] Furthermore, systemic variables such as body mass index (BMI) and renal function profoundly alter circulating protein levels.[13,23,24,] Higher BMI increases total blood plasma volume, artificially diluting NfL concentrations via a hemodilution effect,[13,24] while Reduced renal clearance (reflected by a lower estimated glomerular filtration rate, or eGFR) leads to the systemic accumulation of NfL.[13,23,24] Consequently, applying static, one-size-fits-all cut-offs to unadjusted NfL values inevitably leads to clinical misclassification.

To focus on variations in NfL levels *beyond* normal aging and systemic variations, there is a distinct need for normative modeling. By establishing individualized baseline reference ranges that account for physiological variance, normative modeling transforms a raw biomarker concentration into a standardized estimate (e.g., Z-scores or percentiles) of abnormal, disease-related neuroaxonal injury. This approach has been successfully demonstrated in serum NfL settings, enabling patient-level interpretation of NfL values

relative to expected normative ranges.[14]

With an established biological normative baseline, pathological elevations in plasma NfL, despite its lack of disease specificity, may serve as a useful signal for future neurodegeneration. Evidence indicates that elevated plasma NfL is a promising secondary marker of neuroaxonal injury, potentially signaling microscopic damage that precedes the macroscopic structural brain changes detectable by MRI, such as hippocampal atrophy, cortical thinning, and ventricular enlargement, by several years.[12,22] A clinically practical tool that integrates physiologically adjusted NfL measurements with patient demographics to predict MRI-measured neurodegeneration at the individual level has the potential to bridge a major translational gap.

Once established, these normative model estimates can be tested as predictors of expected neurodegeneration. The primary goal of this project is to apply this normative modeling framework to forecast structural brain health. We hypothesize that baseline plasma NfL measures, once accounted for variance due to normal age and systemic/biological factors, will predict the risk for accelerated MRI-measured neurodegeneration, beyond demographic risk factors and baseline amyloid burden, specifically within a preclinical CU cohort. Such a tool could facilitate proactive monitoring for neurodegeneration suggestive of cognitive decline and imminent symptom onset.

Methods

Data Source and Study Population:

Data were obtained from the Alzheimer's Disease Neuroimaging Initiative (ADNI) database (https://ida.loni.usc.edu), a multi-site longitudinal observational study enrolling cognitively unimpaired (CU), mild cognitive impairment (MCI), and AD dementia participants. Data from the ADNI-1, ADNI-GO, ADNI-2, ADNI-3, and ADNI-4 phases were included. Data was extracted from the ADNI database in June 2026. For each participant, the earliest available visit with a plasma NfL measurement was used as the index (baseline) visit for this cross-sectional analysis; clinical diagnosis, amyloid-PET, APOE genotype, vital signs,

laboratory measures (including eGFR), and structural MRI data corresponding to this index visit were extracted

Cohort Definition and Eligibility Criteria

Plasma NfL measurements were obtained from the ADNI University of Pennsylvania (Upenn) plasma biomarker dataset and were quantified using the Quanterix single molecule array (Simoa) platform. Participants were eligible if they were 55-85 years of age at the index visit and had complete data on plasma NfL, BMI, clinical diagnosis, amyloid-PET status, and APOE genotype. BMI was calculated from height and weight obtained at the index visit; records with missing values, unit inconsistencies, or physiologically implausible values (identified through manual review of source data) were corrected or excluded. Participants missing any required variable were excluded from the analytic sample.

Amyloid-PET Assessment

Amyloid-PET data were derived from ADNI processed PET datasets. Amyloid positivity was defined using tracer-specific standardized uptake value ratio (SUVR) thresholds provided by ADNI (> 1.108 for [18F] florbetapir; > 1.079 for [18F] florbetaben), corresponding approximately to 19 centiloids. Participants were classified as amyloid-positive (Aβ+) or amyloid-negative (Aβ-) accordingly.

Structural MRI

T1-weighted structural MRI and corresponding FreeSurfer-derived regional volumetric measures were obtained from ADNI. Neurodegeneration was characterized using hippocampal volume, AD-signature cortical thickness, and lateral ventricular volume.

Clinical Diagnostic Groups

Clinical diagnosis (CU, MCI, or dementia) was assigned based on ADNI diagnostic summary data at the index visit. The reference group comprised CU Aβ− participants. Four comparator groups were additionally defined: CU Aβ+, MCI Aβ+, dementia Aβ+, and cognitively impaired amyloid-negative participants (MCI or dementia, Aβ-)

Preliminary Analysis of Physiological Determinants

Linear regression analyses were performed within the healthy reference cohort (CU Aβ-) to evaluate associations between plasma NfL and age, BMI, and sex, in order to inform covariate selection for subsequent GAMLSS modeling.

Renal function was evaluated using creatinine-based eGFR. Participants with valid matched eGFR data were stratified into reduced renal function (eGFR<60 mL/min/1.73 m²) and preserved renal function (eGFR ≥ 60 mL/min/1.73 m²) groups. This cutoff corresponds to GFR category G3a or higher in the KDIGO classification system and is commonly used as the clinical threshold for reduced kidney.[25] Extreme eGFR values below 1 mL/min/1.73 m² (range: 0.14-0.47) were identified during distributional quality control as forming a discontinuous cluster clearly separated from the remainder of the eGFR distribution and were excluded as implausible data-quality errors, likely attributable to creatinine unit or data-entry inconsistencies. Baseline characteristics (age, BMI, and plasma NfL concentration) were compared between the reduced and preserved renal function groups using two-sided Wilcoxon rank-sum tests.

GAMLSS Normative Modeling

Given the nonlinear age-related increase and right-skewed distribution of plasma NfL, Generalized Additive Models for Location, Scale, and Shape (GAMLSS; Rigby & Stasinopoulos, 2005) were used to construct normative reference distributions of plasma NfL within the healthy reference cohort (CU Aβ-). Based on the preliminary regression analyses described above, age and BMI were retained as covariates, while sex was excluded. Rather than fitting separate models within each eGFR stratum, eGFR was included as a continuous biological covariate in a single normative model, together with age and BMI.

Plasma NfL was modeled using a Box-Cox t (BCT) distribution to accommodate skewness and heavy tails. The location parameter (μ) was modeled as a smooth function of age, BMI, and eGFR using penalized spline terms:

$$\mu = \beta_0 + s_1(Age) + s_2(BMI) + s_3(eGFR)$$

where β_0 denotes the intercept, and s_1, s_2, and s_3 denote penalized smoothing

functions. The scale and shape parameters (σ, ν, and τ) were modeled as constant across covariates. Models were fitted using the gamlss package in R,[26] adapting code from Preische et al. (2019). Smoothing parameters were estimated automatically by the penalized spline procedure implemented in gamlss.

From the fitted model, plasma NfL percentile curves (1st, 5th, 20th, 50th, 80th, 95th, and 99th percentiles) were derived across the observed age range while holding BMI at representative values of 20, 25, and 30 kg/m², corresponding to low, typical, and elevated BMI levels. To visualize the influence of renal function, percentile curves were additionally plotted with eGFR fixed at the stratum-specific median (52.9 mL/min/1.73 m² for reduced renal function; 80.3 mL/min/1.73 m² for preserved renal function). These strata were used for visualization only; eGFR was modeled as a continuous covariate in the primary GAMLSS model.

Individual NfL Z-scores were calculated using a quantile-based transformation. Each participant's observed NfL concentration was mapped to the fitted conditional cumulative distribution function given their age, BMI, and eGFR, and transformed to the corresponding standard normal quantile:

$$Z = \Phi^{-1}[F(NfL \mid Age, BMI, eGFR)]$$

where F denotes the fitted BCT cumulative distribution function and Φ^{-1} denotes the inverse cumulative distribution function of the standard normal distribution. This approach standardized plasma NfL relative to age-, BMI-, and eGFR-adjusted expectations.

Longitudinal MRI Processing and Harmonization:

Structural MRI measures were obtained from ADNI T1-weighted structural MRI datasets and corresponding FreeSurfer-derived processing outputs. MRI-derived neurodegeneration measures included bilateral hippocampal volume, an AD-signature meta-ROI cortical thickness, and lateral ventricular volume. The AD-signature cortical thickness measure was defined as the average cortical thickness across regions vulnerable to AD-related neurodegeneration, including the entorhinal, inferior temporal, middle temporal, and

fusiform cortices.[27]

Before harmonization, hippocampal and lateral ventricular volumes were adjusted for intracranial volume (ICV) using a residual-based correction approach estimated within CU participants and applied to all eligible MRI scans. AD-signature cortical thickness was not adjusted for ICV. The resulting ICV-adjusted volume measures and cortical thickness measure were subsequently included in the harmonization procedure.

Because ADNI MRI data were acquired across different phases, and because scanner field strength and acquisition protocols evolved systematically over the course of the study, phase and field strength are closely confounded non-biological sources of variance. This may introduce systematic phase effects that confound cross-phase and longitudinal comparisons.[18] To address these effects, MRI measures were harmonized using a ComBat-GAM framework, which models nonlinear covariate effects within a generalized additive model while preserving biologically meaningful variation.[16] ComBat-GAM was fitted using all eligible MRI scans, regardless of plasma NfL availability, clinical diagnosis, or amyloid status, to maximize the sample available for estimating batch effects. A combined categorical variable representing ADNI phase and field strength was used as the batch variable, while age at MRI and sex were included as biological covariates to be preserved during harmonization.

The harmonized MRI measures were subsequently used for W-score construction and longitudinal modeling.

MRI W-score Construction

To quantify MRI abnormality relative to age- and sex-expected values, residual-based MRI W-scores were calculated for hippocampal volume, AD-signature cortical thickness, and lateral ventricular volume. Because the distribution of harmonized MRI measures did not exhibit the pronounced skewness and heavy tails observed in plasma NfL, W-scores were derived using a generalized additive model (GAM) framework with a Gaussian residual structure, rather than the Box-Cox t distribution used for the plasma NfL

normative model.

W-score reference models were constructed using harmonized MRI measures from all eligible participants aged 65–85 years, without restriction by clinical diagnosis or amyloid status. This broader reference sample was selected to align with the full-pool harmonization approach described above and to provide a large, stable reference for the normative GAM models. For each participant in the reference sample, the earliest eligible MRI scan was retained to avoid over-representation of participants with multiple longitudinal scans.

For each MRI outcome, the expected MRI value was estimated using a GAM with age at MRI modeled nonlinearly and sex included as a covariate. MRI W-scores were then calculated as:

$$W = \frac{observed\ harmonized\ MRI\ value - age - and\ ex - predicted\ MRI\ value}{residual\ standard\ deviation\ of\ the\ reference\ model}$$

For hippocampal volume and AD-signature cortical thickness, lower W-scores indicate smaller- or thinner-than-expected brain structure. For lateral ventricular volume, higher W-scores indicate larger-than-expected ventricular volume.

Descriptive MRI Comparisons Across MRI-Anchored Clinical and Amyloid Groups

Prior to formal longitudinal predictive modeling, baseline and longitudinal MRI measures were examined descriptively to characterize structural differences across the disease-stage continuum. Participants were required to have an eligible baseline MRI scan within ±12 months of the plasma NfL measurement, at least one eligible follow-up MRI acquired 2–5 years after baseline, and an age of 65–85 years at MRI acquisition. Clinical diagnosis and amyloid status were defined relative to the baseline MRI. Clinical diagnosis was assigned using the diagnostic assessment nearest to the baseline MRI date. Amyloid-PET records were evaluated relative to the baseline MRI: participants with evidence supporting amyloid positivity at or before baseline, or within one year after baseline, were classified as MRI-anchored Aβ+, whereas those with evidence supporting amyloid negativity within the corresponding temporal window were classified as MRI-anchored Aβ−.

Participants with conflicting or insufficient PET evidence were excluded from the amyloid-defined descriptive groups.

Baseline MRI W-scores and baseline ICV-adjusted, harmonized MRI values were compared between the MRI-anchored CU Aβ− and CU Aβ+ groups using two-sided Wilcoxon rank-sum tests. Individual longitudinal trajectories of the harmonized MRI measures were also plotted for these groups to characterize within-participant change over time. To describe structural abnormality across the broader disease-stage continuum, baseline MRI W-scores and longitudinal W-score trajectories were examined across four MRI-anchored groups: CU Aβ−, CU Aβ+, MCI Aβ+, and dementia Aβ+. For each MRI outcome, two-sided Wilcoxon rank-sum tests were conducted for all pairwise group comparisons, with Benjamini–Hochberg correction for multiple comparisons; only comparisons between adjacent disease stages were displayed in the figures. These analyses were descriptive and were conducted independently of the formal NfL predictive models.

The descriptive MRI cohort did not require a valid physiologically adjusted plasma NfL Z-score. It therefore included 38 CU Aβ+ participants. The primary CU Aβ+ predictive cohort additionally required a valid age-, BMI-, and eGFR-adjusted baseline NfL Z-score; two participants without matched eGFR data were excluded, resulting in 36 participants in the formal linear mixed-effects models.

Longitudinal MRI Cohort Definition

For longitudinal MRI analyses, baseline MRI was defined as the eligible MRI scan closest to the plasma NfL measurement, within a ±12-month window. Follow-up MRI scans were defined as eligible scans acquired 2–5 years after baseline; when multiple follow-up scans were available, all eligible scans within this window were retained for linear mixed-effects modeling. Participants were required to have both a baseline MRI and at least one follow-up MRI within this window.

Because the longitudinal MRI cohort was anchored to the baseline MRI visit rather

than the baseline plasma NfL visit used in the cross-sectional Aβ+/Aβ− classification described above, clinical and amyloid-defined groups for the longitudinal MRI analyses were separately redefined relative to this MRI-anchored baseline. Amyloid-PET records were evaluated relative to the baseline MRI date: participants with PET evidence supporting amyloid positivity at or before baseline, or within 1 year after baseline, were classified as Aβ+ (MRI-anchored Aβ+); participants with PET evidence supporting amyloid negativity within this window were classified as Aβ− (MRI-anchored Aβ−). Participants with conflicting PET evidence or insufficient evidence to determine baseline amyloid status were excluded from the primary amyloid-defined longitudinal MRI groups. Clinical diagnosis was defined using the diagnostic visit nearest to the baseline MRI. The primary longitudinal MRI groups were therefore defined as CU Aβ+ (MRI-anchored) and cognitively impaired Aβ+ (MRI-anchored) participants, with the latter group including MCI and dementia participants classified as Aβ+ at the baseline MRI-defined timepoint.

Longitudinal MRI Prediction Models

To test our hypothesis, linear mixed-effects models were used to evaluate whether baseline plasma NfL Z-score, adjusted for age, BMI, and eGFR, predicted subsequent longitudinal change in MRI W-scores. Separate models were fitted for hippocampal volume W-score, AD-signature cortical thickness W-score, and lateral ventricular volume W-score.

The primary model was specified as:

$$MRI\ W-score \sim Time\ \times\ Baseline\ NfL\ Z-score\ +\ (Time\ |\ Subject)$$

where the Time × Baseline NfL Z-score interaction was the primary term of interest, testing whether higher baseline NfL was associated with faster longitudinal MRI change, and $(Time\ |\ Subject)$ denotes a subject-specific random intercept and random slope for time. Where this random-effects structure resulted in a singular fit or convergence warning, the model was refit using a simplified random-intercept-only structure, $(1\ |\ Subject)$.

Models were fitted separately within CU Aβ+ participants and within a CI Aβ+ group (MCI and dementia), included as a positive-control comparison in which NfL-associated

neurodegeneration was expected to be more readily detectable. Model parameters were estimated in R using restricted maximum likelihood (REML). To account for multiple comparisons across the three MRI outcomes within each cohort, p-values for the $Time \times Baseline\ NfL\ Z-score$ interaction were adjusted using the Benjamini-Hochberg false discovery rate (FDR) procedure. Complete-case analysis was used for each model.

Secondary and exploratory analyses were performed to further evaluate the robustness and biological interpretation of the primary longitudinal findings.

First, an early AD continuum analysis combined CU Aβ+ and MCI Aβ+ participants, given the modest sample size when these groups were analyzed separately. This model retained the same $\boldsymbol{Time \times NfL\ Z-score}$ interaction as the primary term of interest, with clinical stage (CU versus MCI) added as a main-effect covariate to account for differences in average W-score level between the two groups:

$$\boldsymbol{MRI\ W-score \sim Time \times NfL\ Z-score + Clinical\ Stage + (Time \mid Subject)}$$

The clinical stage was not modeled as a time interaction; the model therefore did not separately estimate distinct longitudinal rates of change for CU and MCI participants.

Second, an exploratory longitudinal NfL analysis evaluated whether within-subject change in plasma NfL Z-score, rather than its baseline value alone, was associated with longitudinal MRI W-score change. This analysis was motivated by the possibility that a single baseline NfL measurement may not fully capture the dynamic trajectory of neuroaxonal injury, and that the rate of change in plasma NfL over time could serve as a more sensitive predictor of subsequent structural neurodegeneration than baseline level alone. For participants within the early AD continuum group who had at least two usable longitudinal plasma NfL Z-scores spanning a minimum of 180 days, a participant-specific annualized NfL Z-score slope was first estimated from repeated NfL measurements. This slope was then entered as a subject-level predictor in a separate MRI mixed-effects model:

$$\boldsymbol{MRI\ W-score \sim Time \times NfL\ Z-score\ slope + Clinical\ Stage + (Time \mid Subject)}$$

with the $\boldsymbol{Time \times NfL\ Z-score\ slope}$ interaction as the primary term of interest,

and clinical stage again included as a main-effect covariate. This analysis was considered exploratory given the limited number of participants with repeated NfL measurements available for slope estimation.

Results

Cohort Characteristics

The final analytic sample comprised 971 participants aged 55-85 years who met all eligibility criteria, including valid plasma NfL, BMI, clinical diagnosis, amyloid-PET status, and APOE genotype. The healthy reference group consisted of 388 CU Aβ− participants. Four additional clinical and amyloid-defined comparison groups were included: 176 CU Aβ+, 163 MCI Aβ+, 78 dementia Aβ+, and 166 cognitively impaired Aβ- participants. Cohort characteristics stratified by these groups are shown in Table 1.

Table 1: Cohort Characteristics by Clinical Diagnosis and Amyloid Status

This table summarizes demographic, clinical, genetic, renal-function, and plasma NfL characteristics across the full analytic cohort and the clinical/amyloid-defined subgroups. The healthy control group consisted of cognitively unimpaired (CU), amyloid-negative (Aβ-) participants and served as the reference population for constructing the normative GAMLSS plasma NfL model. The CU Aβ+, MCI Aβ+, and dementia Aβ+ groups represent progressively more advanced stages along the Alzheimer's disease continuum, ranging from preclinical amyloid positivity to symptomatic cognitive impairment and dementia. The CI Aβ− group was included as a comparison group to evaluate cognitive impairment not defined by Aβ+ AD pathology. Across groups, plasma NfL levels were lowest in the healthy control group and higher in Aβ+ and CI groups, supporting the relevance of plasma NfL as a marker of neuroaxonal injury.

Characteristic	Full Analytic Cohort	Healthy Control	CU Aβ+	MCI Aβ+	Dementia Aβ+	CI Aβ-
N	971	388	176	163	78	166
Sex, Female (%)	528 (54.4%)	229 (59.0%)	111 (63.1%)	83 (50.9%)	35 (44.9%)	70 (42.2%)
Age (years), mean (SD)	71.6 (7.1)	69.9 (6.8)	73.4 (6.3)	73.2 (6.4)	73.9 (7.4)	71.2 (7.8)
BMI (kg/m^2), mean (SD)	27.8 (5.6)	28.1 (6.0)	28.4 (6.6)	26.5 (4.5)	26.8 (4.3)	27.9 (5.0)

Characteristic	Full Analytic Cohort	Healthy Control	CU Aβ+	MCI Aβ+	Dementia Aβ+	CI Aβ-
CU	564 (58.1%)	388 (100.0%)	176 (100.0%)	0 (0%)	0 (0%)	0 (0%)
MCI	310 (31.9%)	0 (0%)	0 (0%)	163 (100.0%)	0 (0%)	147 (88.6%)
Dementia	97 (10.0%)	0 (0%)	0 (0%)	0 (0%)	78 (100.0%)	19 (11.4%)
APOE ε4 carrier, n (%)	400 (42.4%)	90 (24.1%)	104 (60.1%)	111 (68.9%)	58 (76.3%)	37 (23.3%)
Amyloid-PET positive, n (%)	417 (42.9%)	0 (0%)	176 (100.0%)	163 (100.0%)	78 (100.0%)	0 (0%)
eGFR, mean (SD)	70.0 (19.3)	72.2 (19.2)	67.2 (18.4)	69.5 (20.0)	64.9 (20.1)	68.2 (19.3)
Plasma NfL, median (pg/mL)	17.3	14.00	17.40	20.70	24.60	17.20
Plasma NfL, mean +/- SD, pg/mL	19.77 +/- 12.95	15.97 +/- 8.84	19.74 +/- 10.81	23.08 +/- 11.75	26.46 +/- 9.93	22.27 +/- 20.62

Preliminary Analysis of Physiological Determinants

Within the healthy reference cohort (CU Aβ−; n = 388), multivariable linear regression analysis (NfL ~ age + BMI + sex) demonstrated that age was significantly associated with higher plasma NfL levels (β = 0.48 pg/mL per year, $P < 0.001$), whereas BMI was significantly associated with lower plasma NfL levels (β = −0.26 pg/mL per kg/m², $P < 0.001$). Sex was not significantly associated with plasma NfL after adjustment for age and BMI (male vs. female: β = 0.23 pg/mL, 95% CI: −1.44 to 1.89, P = 0.789). The corresponding unadjusted associations between plasma NfL and age and BMI are shown in Figure 1. Based on these findings, age and BMI were retained as covariates in the subsequent GAMLSS normative model, whereas sex was excluded because it was not significantly

associated with plasma NfL.

Prior to GAMLSS modeling, descriptive comparisons confirmed that participants with reduced renal function differed systematically from those with preserved renal function across several characteristics relevant to plasma NfL interpretation. Compared with participants with eGFR ≥60 mL/min/1.73m² (*n* = 313), participants with eGFR <60 mL/min/1.73m² (*n* = 65) were older (*P* <0.001), had modestly higher BMI (*P* = 0.032), and had higher plasma NfL concentrations (*P* <0.001; Figure 2). These differences support the inclusion of eGFR as an independent covariate in the GAMLSS normative model, given its association with plasma NfL independent of age and BMI.

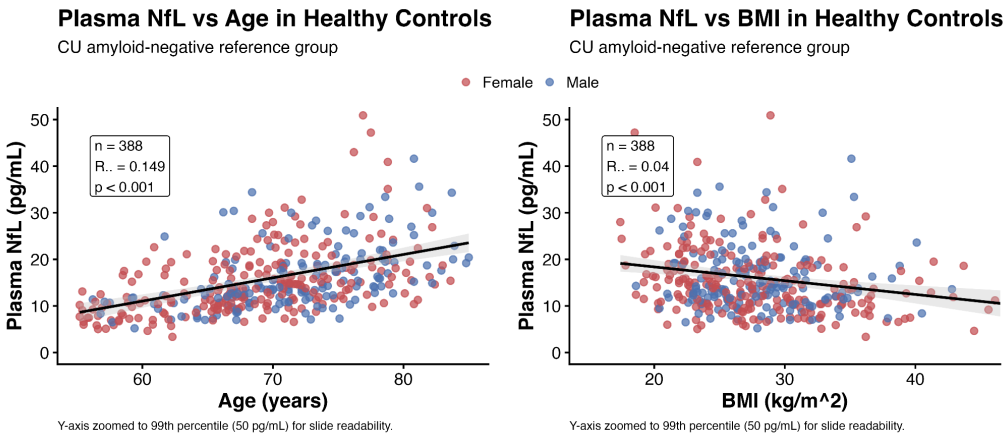

Figure 1: Associations of age and BMI with plasma NfL in the healthy reference cohort

Scatterplots show the associations of plasma NfL concentration with age (A) and BMI (B) among CU Aβ- healthy reference participants (n = 388). Each point represents an individual participant and is colored according to sex. Black lines represent fitted linear regression lines, with shaded areas indicating 95% confidence intervals. The inset boxes report the sample size, coefficient of determination (R²), and P value for each unadjusted association. Age was positively associated with plasma NfL, whereas BMI was inversely associated with plasma NfL. Adjusted associations from the multivariable linear regression model including age, BMI, and sex are reported in the main text.

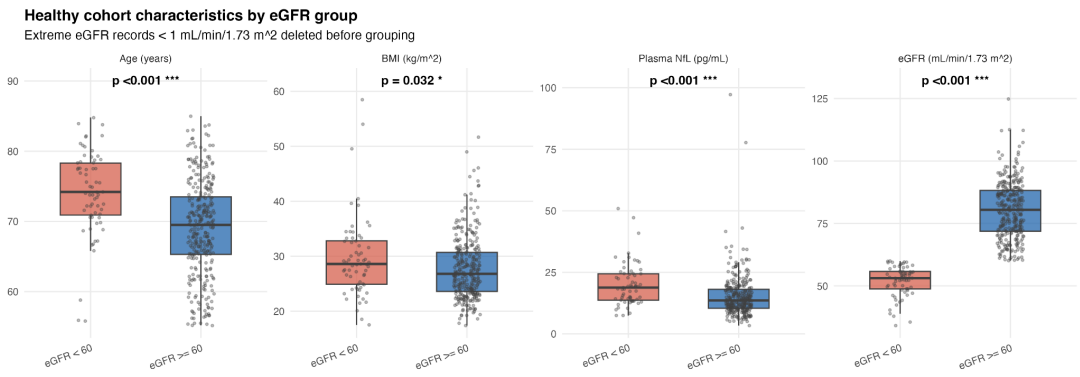

Figure 2: Healthy reference cohort characteristics by renal function group.

Age, BMI, plasma NfL concentration, and eGFR are compared between participants with reduced (eGFR <60 mL/min/1.73m²; n = 65) and preserved (eGFR ≥60 mL/min/1.73m²; n = 313) renal function within the CU, Aβ− healthy reference cohort. Participants with reduced renal function were significantly older (P <0.001), had modestly higher BMI (P = 0.032), and had significantly higher plasma NfL concentrations (P <0.001) than participants with preserved renal function, in addition to the expected eGFR difference defining the two groups (P <0.001). Extreme eGFR values (<1 mL/min/1.73m²) were excluded prior to grouping.

GAMLSS Normative Reference Curves for Plasma NfL

A single GAMLSS normative model was fitted within healthy reference participants with valid matched eGFR data (*n* = 378; CU, amyloid-negative), including 65 participants with reduced renal function (eGFR <60 mL/min/1.73m²) and 313 participants with preserved renal function (eGFR ≥60 mL/min/1.73m²). The Box–Cox t distribution with P-spline smoothers accommodated the right-skewed distribution and heavy tails of plasma NfL while modeling its associations with age, BMI, and eGFR.

As shown in Figure 3, expected plasma NfL concentrations increased progressively with age across all percentile and Z-score levels. The upper percentile curves showed a steeper absolute increase with age than the median and lower percentile curves, resulting in a characteristic "fanning-out" pattern. This pattern indicates that the expected variability of plasma NfL in absolute concentration units increased with advancing age.

BMI showed a consistent inverse association with expected plasma NfL concentrations across the observed age range. At the same age, participants with lower BMI had higher expected plasma NfL values across percentile and Z-score levels, whereas participants with higher BMI had lower expected values. Renal function also influenced the

estimated reference distributions, with lower eGFR associated with higher expected plasma NfL concentrations at the same age and BMI.

Consequently, the absolute plasma NfL concentration corresponding to a given percentile or Z-score varied according to age, BMI, and eGFR. These findings demonstrate that the same observed plasma NfL concentration may represent different degrees of deviation from the healthy reference distribution depending on an individual's demographic and physiological characteristics.

Physiologically adjusted plasma NfL Z-scores, derived from this GAMLSS model, increased progressively across the clinical and amyloid-defined groups (Figure 4, panel A). Compared with the CU Aβ− reference group, median Z-scores were higher in CU Aβ+ (r = 0.14), MCI Aβ+ (r = 0.20, relative to CU Aβ+), dementia Aβ+ (r = 0.20, relative to MCI Aβ+), and CI Aβ− (r = 0.29, relative to dementia Aβ+) participants, with all pairwise comparisons statistically significant (Wilcoxon rank-sum test, P <0.01 for all comparisons; overall Kruskal-Wallis P <0.001).

To evaluate the specific contribution of physiological adjustment, unadjusted Z-scores were also calculated using the same reference group's raw mean and standard deviation, without accounting for age, BMI, or eGFR (Figure 4, panel B). The unadjusted Z-scores pairwise effect sizes that were numerically similar to, and in most comparisons modestly larger than, those observed for the adjusted Z-scores (r = 0.20–0.32 unadjusted versus r = 0.14–0.29 adjusted). Adjustment therefore reduced the magnitude of some pairwise group differences but did not eliminate the clinical/amyloid group pattern, supporting the use of adjusted NfL Z-scores to quantify disease-related NfL elevation beyond expected physiological variation.

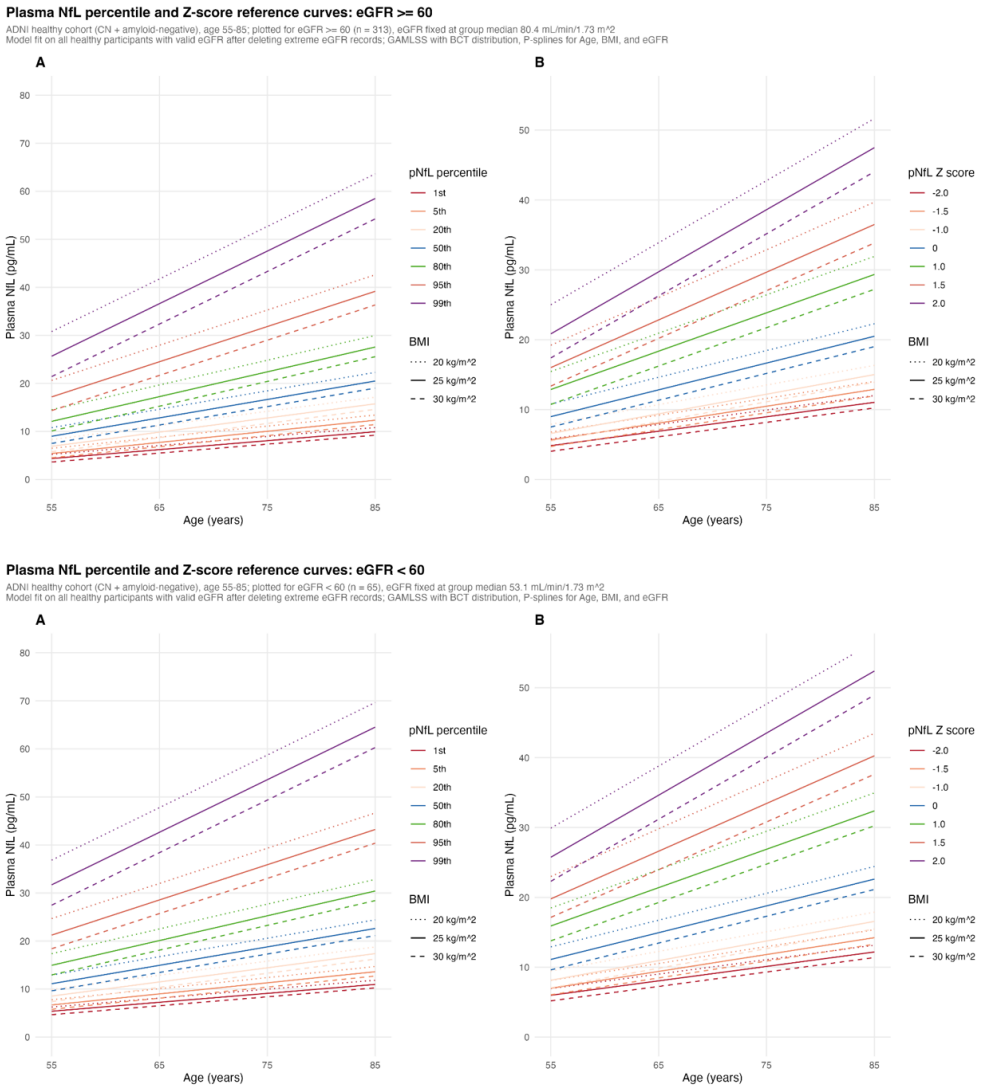

Figure 3: Age-, BMI-, and eGFR-adjusted plasma NfL reference curves derived from GAMLSS

Reference curves were generated from a single Box–Cox t GAMLSS model fitted within healthy reference participants with valid eGFR data (CU, amyloid-negative; n = 378), with age, BMI, and eGFR included as continuous covariates using penalized B-splines. For visualization, eGFR was fixed at the median value within the preserved renal-function group (80.4 mL/min/1.73 m²; panels A and B) and the reduced renal-function group (53.1 mL/min/1.73 m²; panels C and D). 2 Panels A show the estimated 1st, 5th, 20th, 50th, 80th, 95th, and 99th plasma NfL percentiles. 2 Panels B show the absolute plasma NfL concentrations corresponding to Z-scores ranging from −2.0 to 2.0. Curves are presented at BMI values of 20, 25, and 30 kg/m², represented by dotted, solid, and dashed lines, respectively. The eGFR strata were used for visualization only; eGFR was modeled continuously in the primary GAMLSS model.

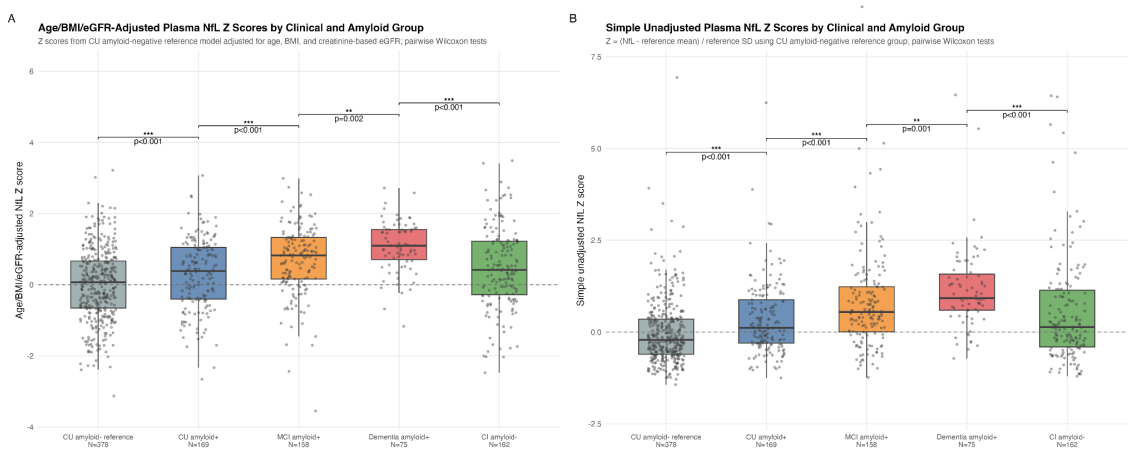

Figure 4: Adjusted and unadjusted plasma NfL Z-scores across clinical and amyloid-defined groups.

(A) Age/BMI/eGFR-adjusted plasma NfL Z-scores, derived from the GAMLSS normative model, and (B) unadjusted plasma NfL Z-scores, calculated as (observed NfL − reference mean) / reference SD, compared across the CU Aβ− reference group (n = 378) and four clinical/amyloid-defined comparison groups: CU Aβ+ (n = 169), MCI Aβ+ (n = 158), dementia Aβ+ (n = 75), and CI Aβ− (n = 162). Between-group comparisons used two-sided Wilcoxon rank-sum tests; effect sizes (r) are shown above each comparison. CI Aβ−, cognitively impaired, amyloid-negative; CU, cognitively unimpaired; MCI, mild cognitive impairment.

MRI Harmonization

Prior to harmonization, all three MRI outcomes showed pronounced, age-independent effects of ADNI phase within the CU Aβ− reference group (Figure 5): hippocampal volume (age-adjusted phase effect, $P = 5.8\times10^{-22}$), lateral ventricular volume ($P = 0.008$), and AD-signature cortical thickness ($P = 1.5\times10^{-68}$). These effects are consistent with systematic non-biological variation associated with differences in field strength, acquisition protocol, and other phase-associated scanner-related factors across the study period.

Following ComBat-GAM harmonization, no significant phase effect remained for any of the three outcomes within this diagnostically homogeneous reference population (Figure 6): hippocampal volume ($P = 0.990$), lateral ventricular volume ($P = 0.986$), and AD-signature cortical thickness ($P = 0.975$). These results indicate that harmonization effectively removed phase-related batch variation across all three neurodegeneration measures while preserving the expected age-related trajectories—declining hippocampal volume and cortical

thickness and increasing ventricular volume—within the healthy reference group.

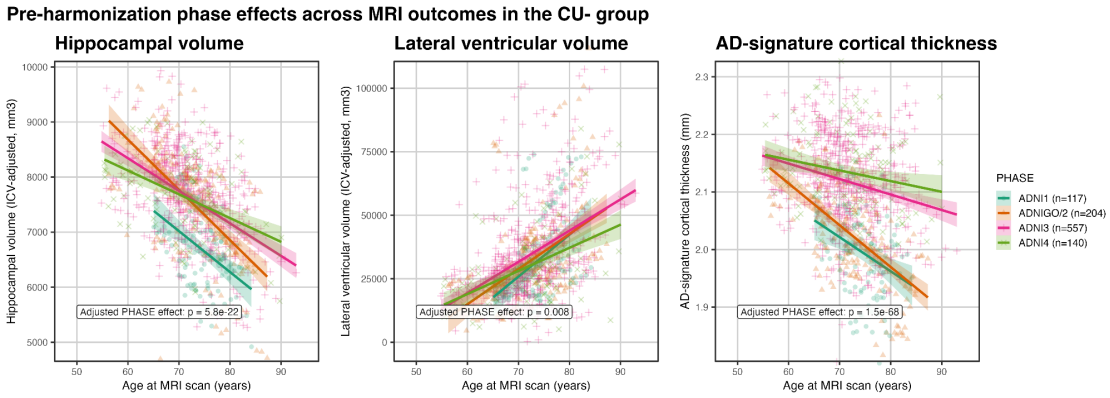

Figure 5: Pre-harmonization phase effects across MRI outcomes in the CU Aβ− reference group.

ICV-adjusted hippocampal volume, lateral ventricular volume, and AD-signature cortical thickness are plotted against age at MRI scan, stratified by ADNI phase, prior to ComBat-GAM harmonization. Pronounced, age-independent phase effects were observed for all three outcomes (age-adjusted phase effect: hippocampal volume, $P = 5.8\times10^{-22}$; lateral ventricular volume, $P = 0.008$; AD-signature cortical thickness, $P = 1.5\times10^{-68}$), consistent with systematic non-biological variation associated with differences in field strength, acquisition protocol, and other phase-associated scanner-related factors.

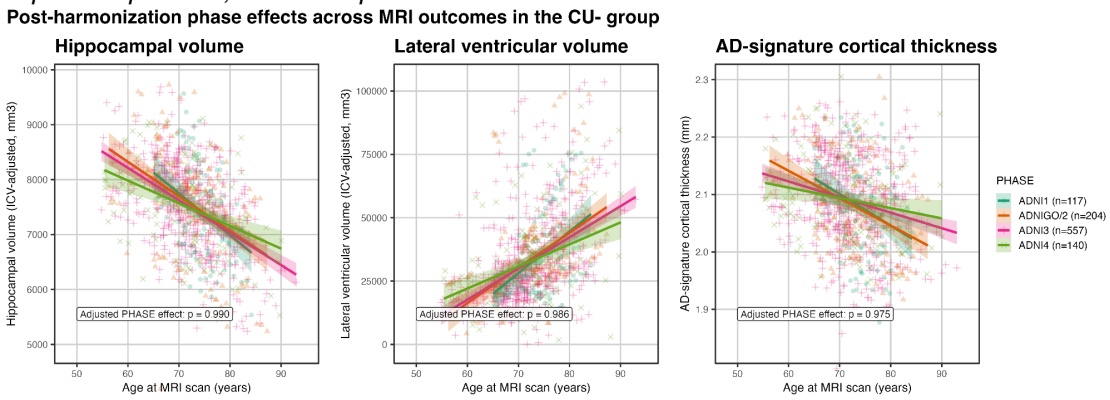

Figure 6: Post-harmonization phase effects across MRI outcomes in the CU Aβ− reference group.

CV-adjusted, ComBat-GAM-harmonized hippocampal volume, lateral ventricular volume, and AD-signature cortical thickness are plotted against age at MRI scan, stratified by ADNI phase, within the same reference group as Figure 5. No significant age-adjusted phase effect remained for any of the three outcomes following harmonization (hippocampal volume, $P = 0.990$; lateral ventricular volume, $P = 0.986$; AD-signature cortical thickness, $P = 0.975$), indicating effective removal of phase-related batch variation while preserving the expected age-related trajectories for each measure.

Longitudinal MRI Cohort Characteristics

The longitudinal CU Aβ+ cohort included 36 participants contributing 77 MRI scans,

and the CI Aβ+ positive-control cohort included 38 participants contributing 87 MRI scans, including 34 participants with MCI and 4 with dementia at baseline. All participants had a baseline MRI and at least one eligible follow-up scan acquired 2–5 years after baseline. Mean follow-up duration was comparable between the two cohorts (CU Aβ+: 3.12 ± 0.84 years; CI Aβ+: 2.93 ± 0.78 years). Most participants contributed two MRI scans, while a smaller proportion contributed three or four scans.

The Early AD Continuum cohort combined the 36 CU Aβ+ participants with the 34 MCI Aβ+ participants, resulting in 70 participants and 155 MRI scans; participants with dementia were not included. The mean follow-up duration was 3.03 ± 0.83 years. The longitudinal NfL analysis was conducted in a subset of 31 Early AD Continuum participants, including 17 CU Aβ+ and 14 MCI Aβ+ participants, who contributed 69 MRI scans. The mean follow-up duration in this subset was 3.07 ± 0.74 years. Individual annualized NfL Z-score slopes were estimated using two or three longitudinal plasma NfL measurements per participant, spanning a mean interval of 4.03 ± 1.74 years. Across all longitudinal analyses, all available eligible MRI observations were retained in the mixed-effects models to account for repeated measurements within participants. Cohort characteristics are summarized in Table 2.

Table 2: Longitudinal MRI Cohort Characteristics

This table summarizes the sample size, clinical composition, number of MRI scans, scan availability per participant, and MRI follow-up duration for the CU Aβ+, cognitively impaired (CI) Aβ+, and longitudinal NfL analysis cohorts. The longitudinal NfL subset included CU Aβ+ and MCI Aβ+ participants with at least two usable plasma NfL measurements. Follow-up duration was calculated from the baseline MRI to the latest eligible follow-up MRI for each participant.

Characteristic	CU Aβ+	CI Aβ+	Early AD Continuum	Longitudinal NfL Subset
Participants, n	36	38	70	31
Diagnosis at baseline	CU Aβ+	MCI: 34; Dementia: 4	CU Aβ+: 36 MCI: 34	CU Aβ+: 17 MCI: 14
Total MRI scans, n	77	87	155	69
Scans per participant, n (%)				
— 2 scans	31 (86.1%)	28 (73.7%)	56 (80.0%)	24 (77.4%)

Characteristic	CU Aβ+	CI Aβ+	Early AD Continuum	Longitudinal NfL Subset
Scans per participant, n (%)				
— 3 scans	5 (13.9%)	9 (23.7%)	13 (18.6%)	7 (22.6%)
— 4 scans	0 (0%)	1 (2.6%)	1 (1.4%)	0 (0%)
Follow-up duration (years), mean ± SD	3.12 ± 0.84	2.93 ± 0.78	3.03 ± 0.83	3.07 ± 0.74
Follow-up duration (years), median (range)	2.98 (2.04–4.89)	2.99 (2.00–4.99)	2.99 (2.00–4.99)	2.99 (2.01–4.29)

Descriptive MRI Findings Across MRI-Anchored Clinical and Amyloid Groups

Baseline MRI W-scores showed numerical differences between the MRI-anchored CU Aβ− and CU Aβ+ groups but did not indicate a consistent pattern of greater structural abnormality among CU Aβ+ participants (Figure 7). Specifically, hippocampal volume and AD-signature cortical thickness W-scores were numerically higher, while lateral ventricular volume W-scores were numerically lower, in the CU Aβ+ group. Given that lower hippocampal and cortical thickness W-scores and higher ventricular W-scores indicate greater abnormality, these findings did not suggest more advanced neurodegeneration in CU Aβ+ participants. Direct comparisons of baseline ICV-adjusted, harmonized MRI values similarly showed no significant group differences in hippocampal volume ($P = 0.718$), AD-signature cortical thickness ($P = 0.237$), or lateral ventricular volume ($P = 0.472$; Figure 8).

Individual longitudinal trajectories showed substantial between-participant variability in both groups (Figure 9). Hippocampal volume generally declined and ventricular volume generally increased over time, whereas changes in cortical thickness were more variable. Overall, visual inspection did not reveal clear separation between the CU Aβ− and CU Aβ+ trajectories.

Across the four MRI-anchored disease-stage groups—CU Aβ− ($n = 126$), CU Aβ+ ($n = 38$), MCI Aβ+ ($n = 35$), and dementia Aβ+ ($n = 4$)—baseline hippocampal volume W-scores were significantly lower in MCI Aβ+ than in CU Aβ+ participants (BH-adjusted $P < 0.001$) and lower in dementia Aβ+ than in MCI Aβ+ participants (BH-adjusted $P = 0.030$; Figure 10). The difference between CU Aβ− and CU Aβ+ participants was not significant

(BH-adjusted $P = 0.209$). No significant adjacent-group differences were observed for AD-signature cortical thickness or lateral ventricular volume W-scores (all BH-adjusted $P > 0.25$).

The longitudinal W-score trajectories were broadly consistent with these baseline findings (Figure 11). Hippocampal W-scores appeared lower and showed clearer decline in the symptomatic MCI Aβ+ and dementia Aβ+ groups, whereas separation across disease stages was less evident for cortical thickness and ventricular volume. Because the dementia Aβ+ group included only four participants, its apparent baseline and longitudinal patterns should be interpreted cautiously.

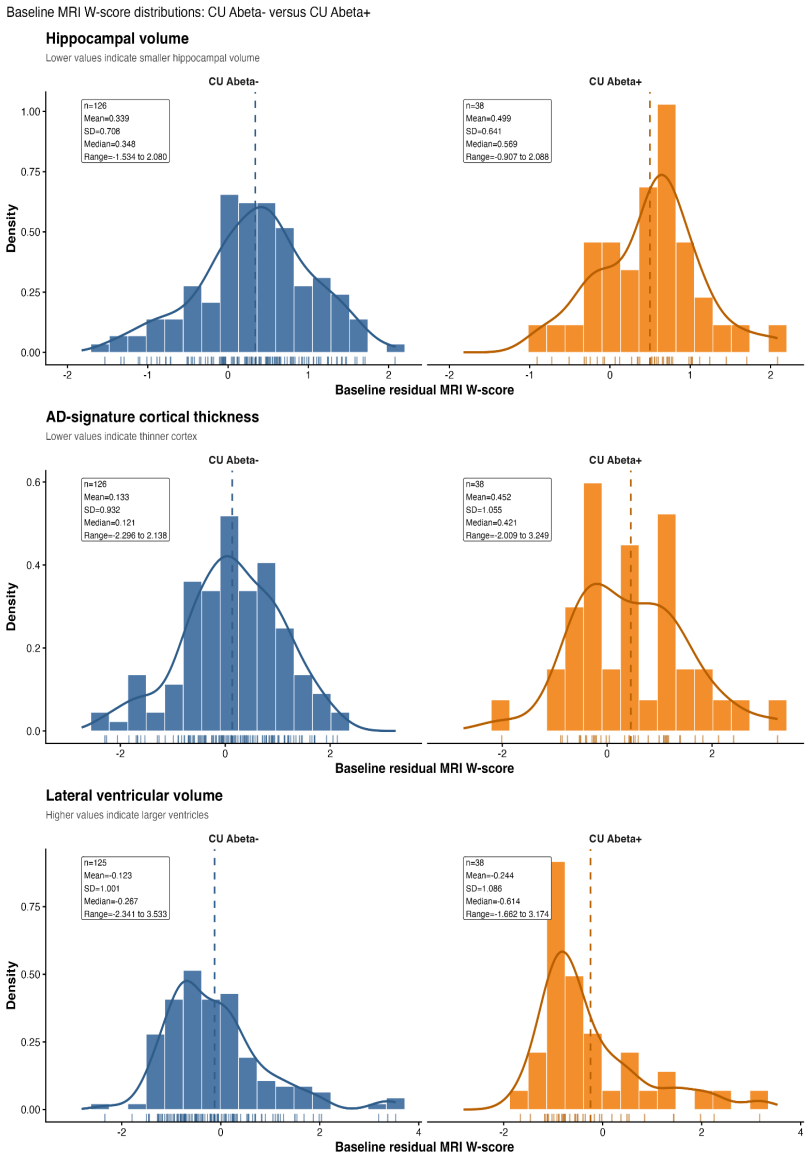

Figure 7: Baseline MRI W-score distributions: CU Aβ− versus CU Aβ+.
Distributions of baseline MRI W-scores for hippocampal volume, AD-signature cortical thickness, and lateral ventricular volume are shown for the CU, amyloid-negative reference group and the CU Aβ+ descriptive cohort (n = 38). Clinical diagnosis and amyloid-PET status were defined relative to the baseline plasma NfL visit (plasma-anchored classification). Dashed lines indicate group means.

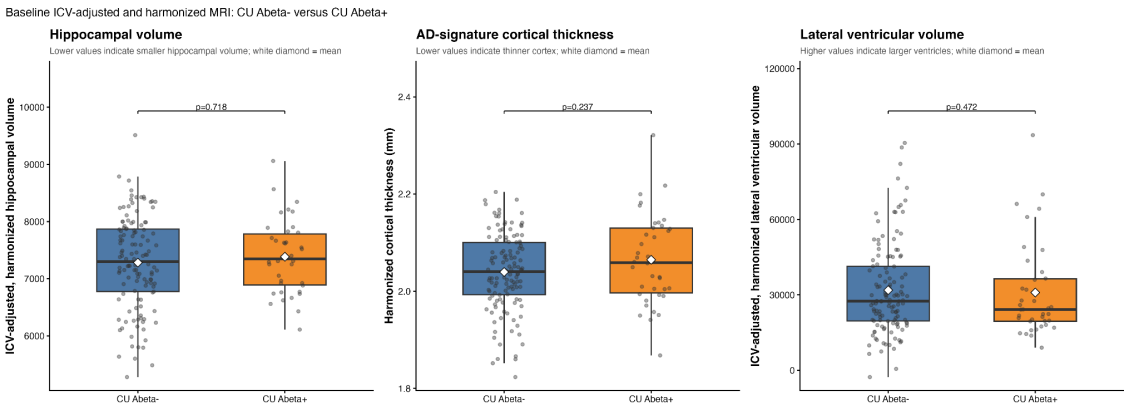

Figure 8: Baseline ICV-adjusted, harmonized MRI values: CU Aβ− versus CU Aβ+. *ICV-adjusted, ComBat-GAM-harmonized baseline MRI values are compared between the CU, amyloid-negative reference group and the CU Aβ+ descriptive cohort (n = 38) for hippocampal volume, AD-signature cortical thickness, and lateral ventricular volume. White diamonds indicate group means. Between-group comparisons used two-sided Wilcoxon rank-sum tests; none of the three comparisons reached statistical significance.*

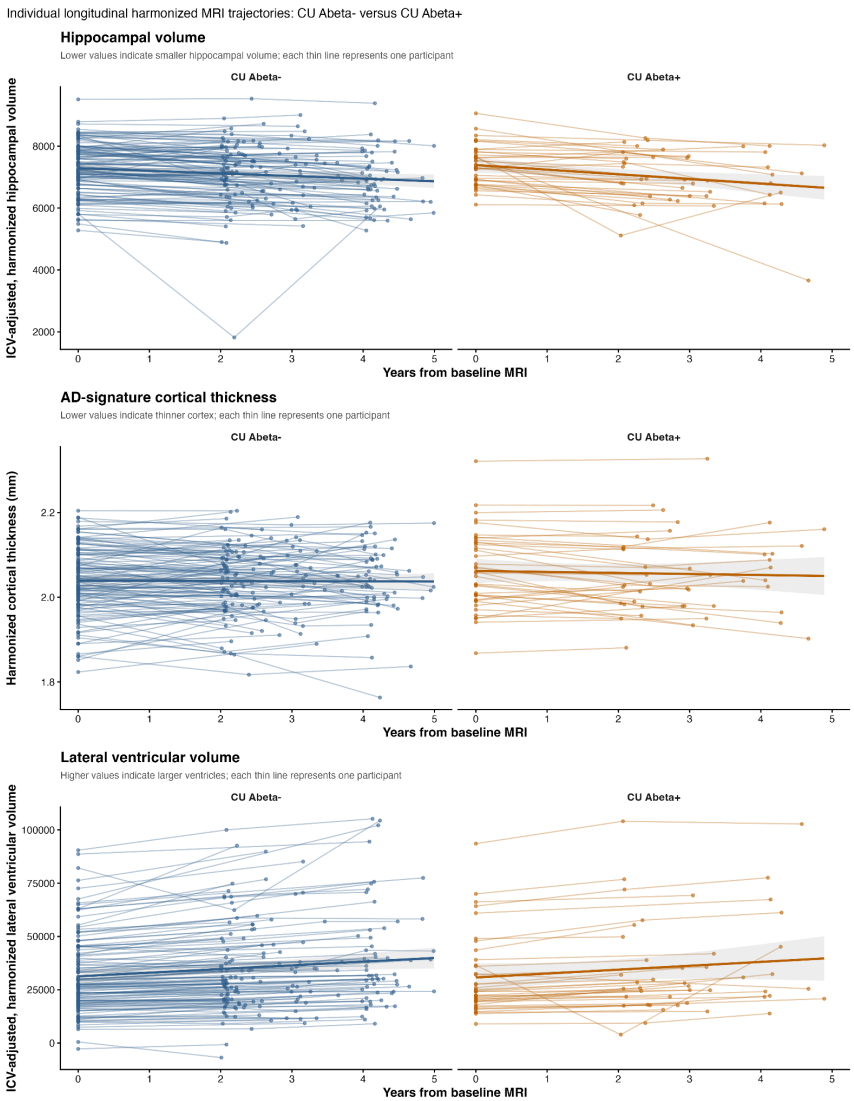

Figure 9: Individual longitudinal harmonized MRI trajectories: CU Aβ− versus CU Aβ+. *Individual participant trajectories of ICV-adjusted, ComBat-GAM-harmonized MRI values are shown over time from baseline MRI for the CU, amyloid-negative reference group and the CU Aβ+ descriptive cohort. Thin lines represent individual participants; thick lines represent the fitted group-level trend. These trajectories are descriptive and were not accompanied by formal statistical testing.*

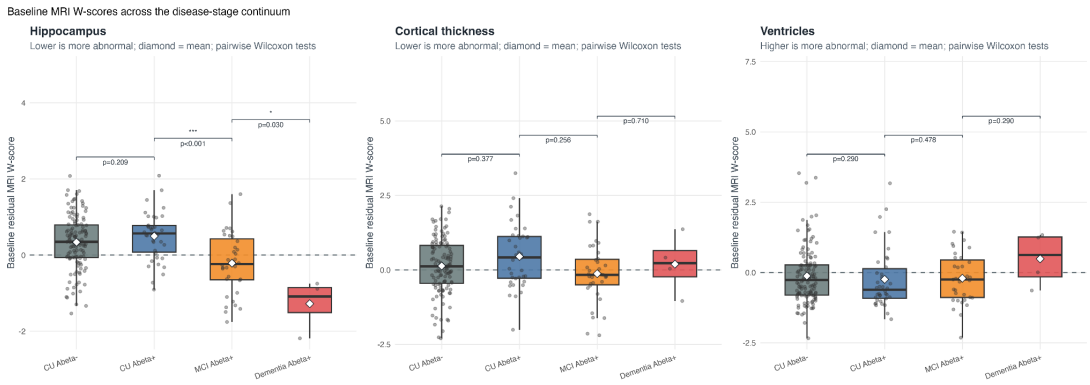

Figure 10: Baseline MRI W-scores across the disease-stage continuum. *Individual participant trajectories of MRI W-scores are shown over time from baseline MRI for hippocampal volume, AD-signature cortical thickness, and lateral ventricular volume, stratified by clinical/amyloid group as defined relative to the baseline plasma NfL visit (CU Aβ−, CU Aβ+, MCI Aβ+, dementia Aβ+). Thin blue lines represent individual participants; the orange line represents the descriptive group-level trend with 95% confidence band. These trajectories are descriptive and were not accompanied by formal statistical testing.*

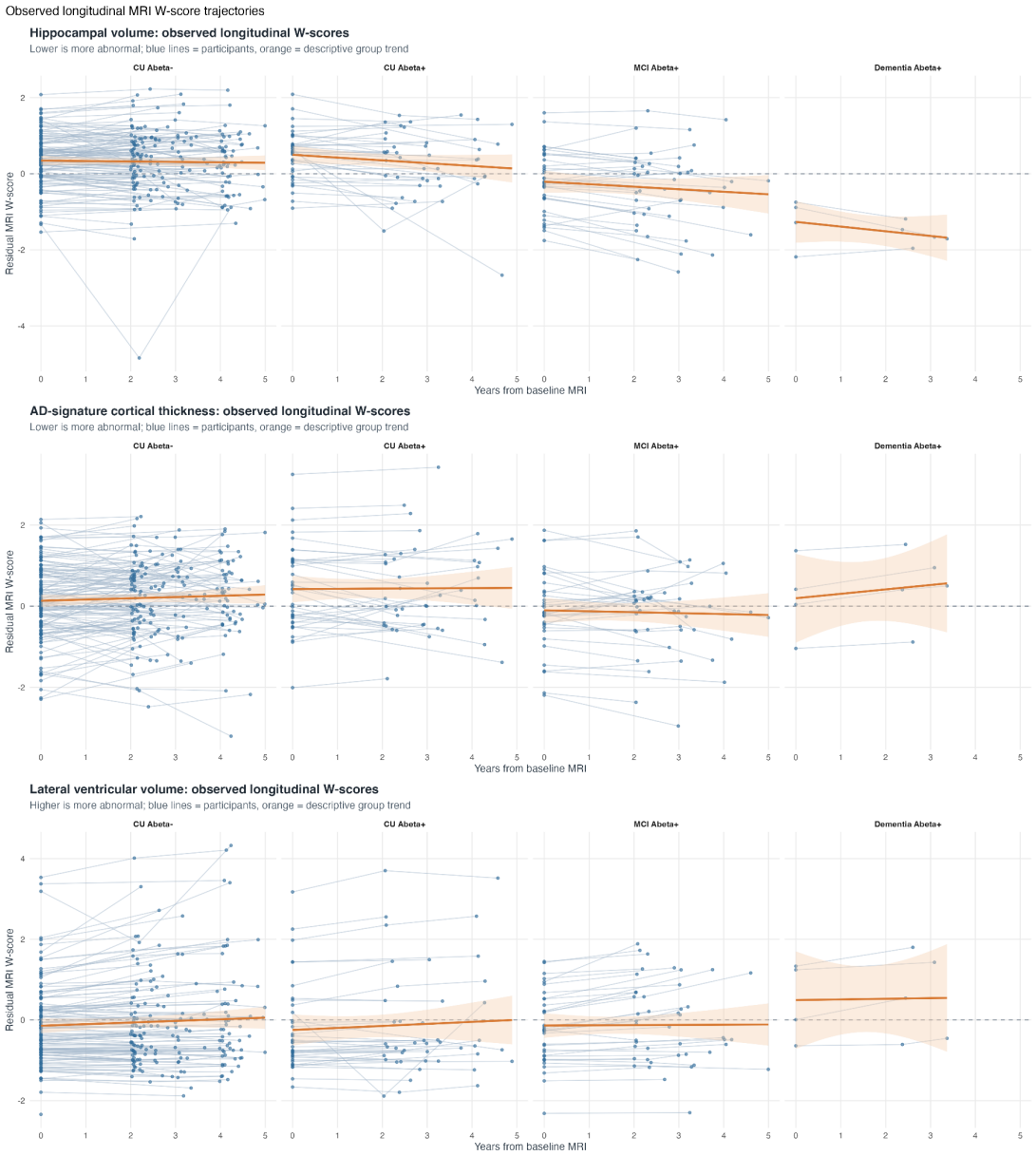

Figure 11: Observed longitudinal MRI W-score trajectories across the disease-stage continuum.

Individual participant trajectories of MRI W-scores are shown over time from baseline MRI for hippocampal volume, AD-signature cortical thickness, and lateral ventricular volume, stratified by MRI-anchored clinical and amyloid-defined group (CU Aβ−, CU Aβ+, MCI Aβ+, dementia Aβ+). Thin blue lines represent individual participants; the orange line represents the descriptive group-level trend with 95% confidence band. These trajectories are descriptive and were not accompanied by formal statistical testing.

Longitudinal Predictive Modeling: Baseline nfL Z-score and MRI W-score Trajectories

In the primary CU Aβ+ cohort, baseline plasma NfL Z-score was not significantly associated with longitudinal change in any of the three MRI W-scores (Figure 12). The Time × Baseline NfL Z-score interaction was not significant for hippocampal volume (β = −0.001,

P = 0.975), AD-signature cortical thickness (*β* = −0.010, *P* = 0.729), or lateral ventricular volume (*β* = 0.017, *P* = 0.234). Although the interaction estimates were generally in the expected directions, their magnitudes were small, and the model-estimated trajectories did not provide evidence that higher baseline plasma NfL Z-scores predicted faster subsequent MRI change in CU Aβ+ participants.

Within the CI Aβ+ positive-control cohort, baseline plasma NfL Z-score was also not significantly associated with longitudinal change in any MRI W-score (Figure 13). The Time × Baseline NfL Z-score interaction was not significant for hippocampal volume (*β* = 0.038, *P* = 0.295), AD-signature cortical thickness (*β* = −0.022, *P* = 0.628), or lateral ventricular volume (*β* = −0.031, *P* = 0.247). Thus, the positive-control analysis did not demonstrate evidence that higher baseline plasma NfL Z-scores predicted faster subsequent MRI change among CU Aβ+ participants.

Similarly, in the Early AD Continuum cohort, which combined CU Aβ+ and MCI Aβ+ participants, baseline plasma NfL Z-score was not significantly associated with longitudinal change in hippocampal volume (*β* = 0.010, *P* = 0.664), AD-signature cortical thickness (*β* = −0.018, *P* = 0.456), or lateral ventricular volume W-score (*β* = 0.011, *P* = 0.446; Figure 14). Although the interaction estimates for cortical thickness and lateral ventricular volume were in the expected directions, none reached statistical significance.

In the exploratory longitudinal NfL analysis, a greater annualized increase in plasma NfL Z-score was associated with a faster decline in hippocampal volume W-score (Time × NfL Z-score slope: *β* = −0.225, *P* = 0.045; Figure 15). The corresponding interaction estimates for AD-signature cortical thickness (*β* = −0.162, *P* = 0.201) and lateral ventricular volume (*β* = 0.115, *P* = 0.178) were also in the expected directions but were not statistically significant. After adjustment for multiple comparisons across the three MRI outcomes, the association with hippocampal volume did not remain significant (FDR-adjusted *P* = 0.135).

Overall, a single baseline plasma NfL Z-score was not significantly associated with subsequent MRI W-score trajectories in the CU Aβ+, CI Aβ+, or Early AD Continuum cohorts. The exploratory longitudinal NfL analysis suggested that increases in plasma NfL

over time may be more closely related to concurrent hippocampal volume decline than a single baseline measurement; however, this finding did not remain significant after correction for multiple comparisons.

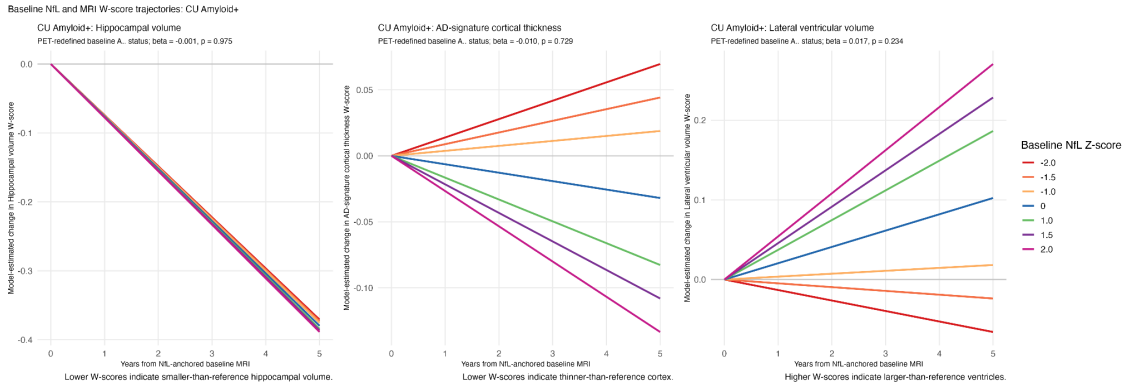

Figure 12. Baseline Plasma NfL Z-score and Longitudinal MRI W-score Trajectories in CU Aβ+ Participants

Model-estimated changes in hippocampal volume, AD-signature cortical thickness, and lateral ventricular volume W-scores are shown across selected baseline plasma NfL Z-scores. Hippocampal trajectories largely overlapped, while modest separation was observed for cortical thickness and ventricular volume. However, the Time × Baseline NfL Z-score interaction was not significant for hippocampal volume (β = −0.001, P = 0.975), cortical thickness (β = −0.010, P = 0.729), or ventricular volume (β = 0.017, P = 0.234), indicating that baseline NfL did not significantly predict MRI W-score change in CU Aβ+ participants.

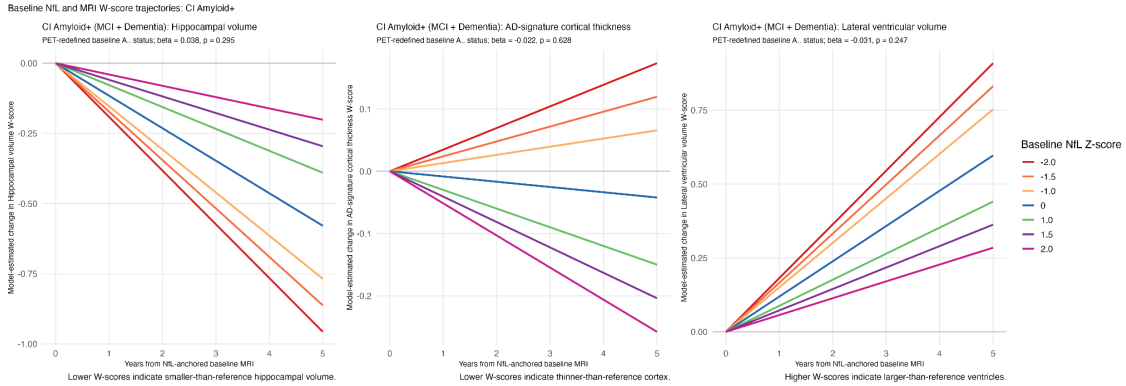

Figure 13. Baseline Plasma NfL Z-score and Longitudinal MRI W-score Trajectories in CI Aβ+ Participants

Model-estimated MRI W-score trajectories are shown across selected baseline plasma NfL Z-scores in the CI Aβ+ positive-control cohort. The directions of the estimated associations varied across the three MRI outcomes, and no consistent pattern of greater neurodegeneration at higher baseline NfL Z-scores was observed. The Time × Baseline NfL Z-score interaction was not significant for hippocampal volume (β = 0.038, P = 0.295), cortical thickness (β = −0.022, P = 0.628), or ventricular volume (β = −0.031, P = 0.247).

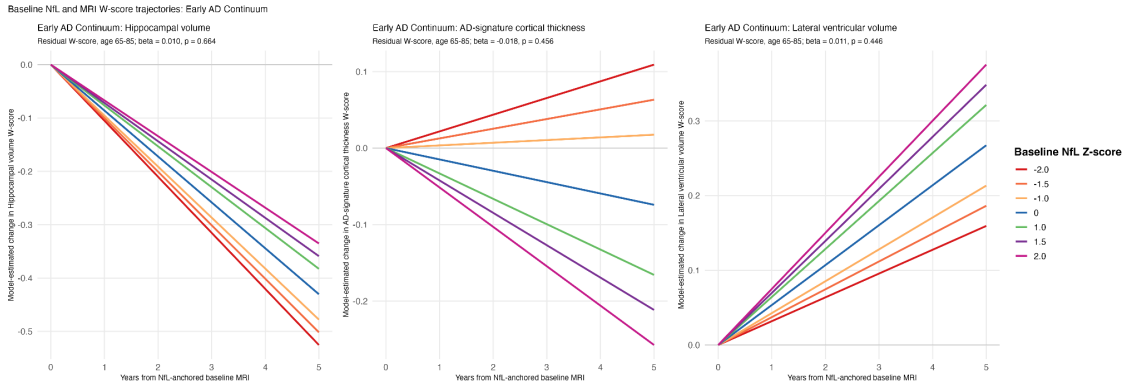

Figure 14. Baseline Plasma NfL Z-score and Longitudinal MRI W-score Trajectories in the Early AD Continuum

Model-estimated MRI W-score trajectories are shown across selected baseline plasma NfL Z-scores in the Early AD Continuum cohort, which included CU Aβ+ and MCI Aβ+ participants. Higher baseline NfL Z-scores corresponded to estimated trajectories toward greater cortical thinning and ventricular enlargement, whereas this pattern was not observed for hippocampal volume. Nevertheless, the Time × Baseline NfL Z-score interaction was not significant for hippocampal volume (β = 0.010, P = 0.664), cortical thickness (β = −0.018, P = 0.456), or ventricular volume (β = 0.011, P = 0.446). Clinical stage was included as a covariate.

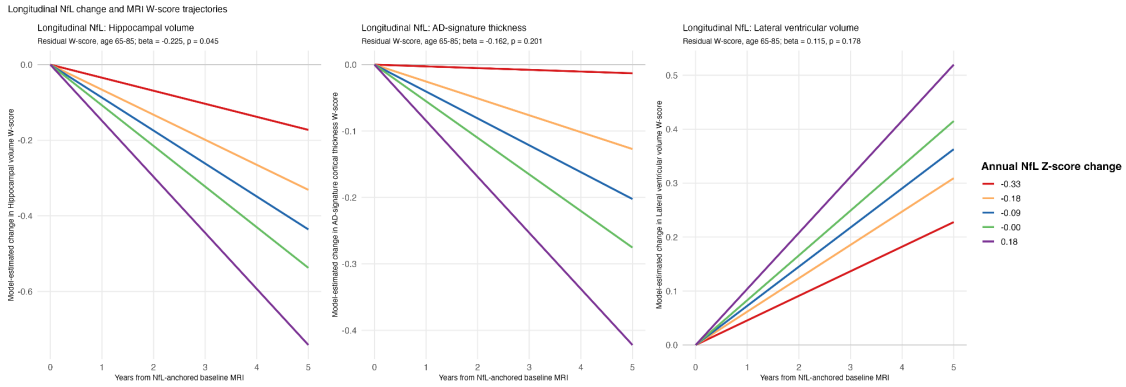

Figure 15. Longitudinal Plasma NfL Change and MRI W-score Trajectories in the Early AD Continuum

Model-estimated MRI W-score trajectories are shown according to selected participant-specific annualized plasma NfL Z-score slopes in the longitudinal NfL subset. Greater annualized increases in NfL Z-score corresponded to faster hippocampal volume decline and directionally greater cortical thinning and ventricular enlargement. The Time × NfL Z-score Slope interaction was significant for hippocampal volume before multiple-comparison correction (β = −0.225, P = 0.045), but not for cortical thickness (β = −0.162, P = 0.201) or ventricular volume (β = 0.115, P = 0.178). The hippocampal association did not remain significant after FDR correction (PFDR = 0.135). Clinical stage was included as a covariate.

Discussion

This study developed individualized plasma NfL reference distributions adjusted for

age, BMI, and renal function and evaluated whether the resulting NfL Z-scores predicted longitudinal MRI-measured neurodegeneration across amyloid-positive stages of AD. Plasma NfL increased with age, decreased with higher BMI, and was higher among participants with lower eGFR. After accounting for these physiological factors, plasma NfL Z-scores showed a graded increase from the CU Aβ− reference group to CU Aβ+, MCI Aβ+, and dementia Aβ+ participants, supporting the biological relevance of the normative model. Cross-sectional comparisons of MRI-derived measures across the same clinical and amyloid-defined continuum provided partial corroborating evidence. Baseline hippocampal volume W-scores declined significantly with advancing disease stage, whereas AD-signature cortical thickness and lateral ventricular volume did not differ significantly across adjacent stages, suggesting that hippocampal volume may have been more responsive to cross-sectional differences in disease stage than the other two structural measures in this cohort. However, a single baseline plasma NfL Z-score was not significantly associated with subsequent change in hippocampal volume, AD-signature cortical thickness, or lateral ventricular volume W-score in the CU Aβ+, CI Aβ+, or Early AD Continuum cohorts. In the exploratory longitudinal NfL analysis, a greater annualized increase in NfL Z-score was associated with faster hippocampal volume decline before multiple-comparison correction, although this association did not remain significant after FDR adjustment. Together, these findings suggest that physiologically adjusted NfL Z-scores can characterize group-level differences in neuroaxonal injury across the AD continuum, while longitudinal NfL change warrants further investigation as a potentially more informative marker of ongoing structural neurodegeneration than a single baseline measurement.

The observed associations of age, BMI, and eGFR with plasma NfL support the need to account for normal biological and systemic variation when interpreting this biomarker. Plasma NfL increased with age, consistent with previous evidence that NfL levels rise during normal aging and are associated with age-related brain changes.20 The GAMLSS reference curves also showed progressively greater absolute variability at older ages, particularly at the upper percentiles. This widening of the reference distribution indicates that a fixed

increase in plasma NfL does not have the same meaning across the adult age range. An NfL concentration considered elevated in a younger individual may fall within the expected distribution for an older individual, emphasizing the limitations of applying a universal concentration threshold.

BMI showed an inverse association with plasma NfL, consistent with the proposed hemodilution effect.13,24 Individuals with higher BMI generally have a larger blood volume, which may reduce the measured concentration of circulating NfL without reflecting less neuroaxonal injury. Failure to account for BMI could therefore lead to underestimation of NfL abnormality in individuals with higher BMI. Renal function also influenced the estimated reference distributions, with lower eGFR associated with higher expected plasma NfL concentrations.13,23,24 Reduced renal clearance has been proposed as one possible contributor to the systemic accumulation of NfL or related protein fragments, producing higher measured concentrations independent of central nervous system pathology. Modeling eGFR as a continuous covariate allowed the expected NfL distribution to vary across the observed range of renal function without excluding participants solely on the basis of a clinical eGFR threshold. Collectively, these findings indicate that the same observed NfL concentration may represent different degrees of neuroaxonal injury depending on an individual's age, BMI, and renal function.

After physiological adjustment, plasma NfL Z-scores retained a graded increase across clinical and amyloid-defined stages of AD. This group-level pattern is consistent with increasing neuroaxonal injury across advancing disease stages and provides initial evidence that the normative model retained clinically meaningful biological variation. Importantly, the adjustment did not remove the expected differences between clinical and amyloid-defined groups. Nevertheless, substantial overlap remained between the distributions. Therefore, although the NfL Z-score provides a standardized measure of neuroaxonal injury relative to physiologically expected values, it should not be interpreted as an AD diagnostic measure or used alone to classify an individual's clinical stage.

In the primary longitudinal analysis, baseline plasma NfL Z-score did not significantly

predict MRI W-score change in CU Aβ+ participants. The interaction estimates for hippocampal volume, AD-signature cortical thickness, and lateral ventricular volume were generally in the expected directions, but their magnitudes were small and none reached statistical significance. These results do not provide sufficient evidence that a single physiologically adjusted NfL measurement can identify which cognitively unimpaired amyloid-positive individuals will experience faster structural neurodegeneration over the subsequent two to five years. Although visual separation was observed among some of the model-estimated trajectories, these patterns should be interpreted cautiously in the absence of statistically supported interactions.

The CI Aβ+ cohort was included as a positive-control analysis because the relationship between neuroaxonal injury and structural neurodegeneration was expected to be more detectable during symptomatic disease. However, baseline NfL Z-score was also not significantly associated with any MRI W-score trajectory in this cohort, and the directions of the interaction estimates were not consistent across outcomes. This analysis was subject to the same methodological constraints as the CU Aβ+ cohort, including a modest sample size, limited repeated MRI observations, and a comparatively short follow-up window. It may therefore not have provided sufficient power to detect an association during symptomatic disease. The null positive-control result is consistent with two distinct interpretations: baseline NfL may not predict short-term structural change even in symptomatic AD, or the analysis may have lacked adequate power to detect such an association regardless of disease stage. The present data cannot fully distinguish between these possibilities.

Similarly, combining CU Aβ+ and MCI Aβ+ participants into the Early AD Continuum increased the available sample but did not produce significant associations between baseline NfL Z-score and longitudinal MRI change. The absence of significant associations despite the larger sample suggests that the additional observations were insufficient to overcome other sources of variability. Combining participants across the preclinical-to-prodromal transition may have introduced disease-stage heterogeneity in the rate and pattern of neurodegeneration, offsetting the statistical benefit of the larger cohort. Higher

baseline NfL Z-scores were accompanied by model-estimated trends toward greater cortical thinning and ventricular enlargement, although these interactions remained statistically uncertain. Collectively, the positive-control and Early AD Continuum analyses indicate that the CU Aβ+ null result cannot be attributed solely to a weaker neurodegenerative signal during the preclinical stage.

In contrast to the baseline analyses, the exploratory longitudinal NfL analysis raised the possibility that within-person NfL change may be more closely related to ongoing structural neurodegeneration. A greater annualized increase in plasma NfL Z-score was associated with faster hippocampal volume W-score decline. The interaction reached nominal statistical significance but did not remain significant after correction for the three MRI outcomes. The estimated associations for AD-signature cortical thickness and lateral ventricular volume were also in the expected directions but were not significant. This pattern is consistent with previous evidence that longitudinal NfL dynamics are associated with neurodegeneration and clinical progression.12,22 A single NfL measurement reflects both stable between-person differences and neuroaxonal injury at one point in time, whereas repeated measurements may better identify an active increase beyond an individual's previous level. Longitudinal NfL change may therefore warrant further investigation as a potentially more sensitive marker of ongoing disease activity than a single baseline value.

The hippocampal finding is biologically plausible because hippocampal atrophy is an established structural feature of AD and may be detectable during the transition from preclinical to symptomatic disease. However, this result should be considered hypothesis-generating rather than confirmatory. The longitudinal NfL subset included only 31 participants, each contributing two or three usable NfL measurements, and the association did not remain significant after FDR correction. Participant-specific NfL slopes estimated from a small number of measurements may also be sensitive to assay variability, short-term physiological fluctuations, and the timing of blood collection. The result therefore suggests a potential relationship that warrants further investigation rather than confirming that longitudinal NfL change independently predicts hippocampal atrophy.

Several biological factors may explain why baseline NfL Z-score did not reliably predict subsequent MRI change. First, NfL is a sensitive but nonspecific marker of neuroaxonal injury.7,8 Elevated NfL may reflect AD-related neurodegeneration, but it can also be influenced by cerebrovascular disease, other neurological disorders, systemic illness, or acute neuronal injury. Consequently, an elevated NfL Z-score does not necessarily indicate that AD-related structural atrophy will occur during the subsequent observation period. Second, NfL elevation may precede MRI-detectable structural changes.2 This may create a temporal mismatch between a single baseline NfL measurement and the relatively short subsequent MRI follow-up period. Some participants may have experienced NfL elevation before the selected baseline, whereas corresponding structural changes may have occurred before baseline or may emerge after the available follow-up window. Third, Aβ+ participants are heterogeneous in tau burden, vascular comorbidity, cognitive reserve, disease duration, and proximity to symptom onset. Amyloid positivity alone may therefore be insufficient to identify individuals undergoing active and measurable neurodegeneration during a particular follow-up period.

The pattern observed in the cross-sectional MRI comparisons further contextualizes the exploratory longitudinal NfL result. Hippocampal volume was the only outcome to show a statistically significant cross-sectional gradient across disease stages, and it was also the only outcome for which longitudinal NfL change showed a nominally significant association. This convergence raises the possibility that hippocampal volume may be a particularly responsive structural correlate of neuroaxonal injury within this cohort and follow-up period, consistent with the relatively early and pronounced involvement of the hippocampus in AD-related neurodegeneration. However, this pattern remains hypothesis-generating given the descriptive nature of the cross-sectional comparisons, the small dementia Aβ+ group, and the limited longitudinal NfL sample.

One counterintuitive observation in the cross-sectional comparison was that CU Aβ+ participants showed numerically higher, or less abnormal, hippocampal volume W-scores than the CU Aβ− reference group, although this difference was not statistically significant (*P*

= 0.209). This pattern likely reflects the descriptive, cross-sectional nature of the comparison rather than a protective effect of amyloid positivity. Possible contributing factors include the modest and potentially selected sample of amyloid-positive individuals who remained cognitively unimpaired, selection effects among individuals who had not yet progressed, and sampling variability given the group sizes. Individuals who remain cognitively unimpaired despite amyloid positivity may also have greater cognitive or structural reserve. This observation underscores that a single cross-sectional snapshot cannot capture the trajectory of neurodegeneration and reinforces the importance of evaluating structural change longitudinally.

The present study also has several methodological limitations. The longitudinal cohorts were modest in size, including 36 CU Aβ+ participants, 38 CI Aβ+ participants, and 70 participants in the Early AD Continuum analysis. The cross-sectional disease-stage comparisons were also limited by small subgroup sizes, with only four participants in the dementia Aβ+ group. The statistically significant hippocampal volume difference between the MCI Aβ+ and dementia Aβ+ groups should therefore be interpreted with particular caution because estimates based on so few participants are highly sensitive to individual data points. The longitudinal NfL subset was further reduced to 31 participants.

Most participants contributed only two MRI scans, with relatively few contributing three or four scans. When only two observations are available, estimated individual change is highly sensitive to measurement variability, and nonlinear trajectories cannot be evaluated. The limited number of repeated observations also reduced support for subject-specific random slopes, resulting in simplified random-intercept models when the full random-effects structure produced singular fits or convergence warnings. Although mixed-effects models retained all available observations and accounted for repeated measurements within participants, larger cohorts with more densely sampled MRI data would provide more reliable estimates of individual change and greater power to detect NfL-associated differences in trajectories.

The construction of the MRI W-scores should also be considered when interpreting

the longitudinal findings. The MRI reference models were fitted using all eligible participants aged 65–85 years, without restriction by clinical diagnosis or amyloid status. The resulting W-scores therefore represent age- and sex-adjusted deviations relative to a broad ADNI MRI population rather than abnormalities relative to a strictly healthy reference group. This approach provided a large and stable reference sample but may have reduced the contrast between normal and disease-related structural variation. It also introduced a scale mismatch between the two biomarkers under study: plasma NfL Z-scores were referenced strictly against a CU Aβ− population, whereas MRI W-scores were referenced against a broader, diagnostically heterogeneous population. This difference in reference frameworks may have affected the magnitude and interpretation of their estimated association independently of the underlying biological relationship. Future analyses should compare the current W-scores with those derived from a comparably defined CU Aβ− reference sample.

In addition, ComBat-GAM was used to reduce major phase- and field-strength-related differences while preserving age- and sex-associated variation.16 However, methods specifically designed for longitudinal harmonization may better account for dependence between repeated scans and preserve within-subject change. The exploratory longitudinal NfL analysis also used a two-stage procedure in which an annualized NfL Z-score slope was first estimated for each participant and then entered as a subject-level predictor in the MRI mixed-effects model. This approach does not fully account for uncertainty in the estimated NfL slopes, which is particularly important when slopes are based on only two or three measurements. Joint longitudinal models or time-varying NfL predictors may provide more appropriate alternatives when denser repeated measurements are available.

Additional limitations relate to the normative model and generalizability. Although the healthy reference sample with complete eGFR data was sufficient for primary GAMLSS estimation, the 95th and 99th percentiles may be less stable because they are estimated from relatively few observations, particularly at the youngest and oldest ages and among participants with reduced renal function. The observational design also prevents causal interpretation of the associations. In addition, ADNI participants are not fully representative

of the general older population and have limited racial, ethnic, socioeconomic, and clinical diversity. Physiological factors affecting NfL and patterns of MRI change may differ in populations with a greater burden of renal, cardiovascular, or neurological comorbidities. External validation in larger and more diverse cohorts is therefore required before these reference distributions or predictive models can be considered for clinical application.

Future studies should prioritize larger Aβ+ cohorts with more frequent and closely synchronized plasma NfL and MRI measurements over longer follow-up periods. Repeated measurements would permit more reliable estimation of biomarker and imaging trajectories and allow investigation of nonlinear change. With sufficient data, latent class mixed modeling could be used to identify subgroups with distinct patterns of structural decline and to test whether baseline or longitudinal NfL predicts membership in a rapid-atrophy trajectory. Multivariate mixed-effects models could also jointly analyze hippocampal volume, cortical thickness, and ventricular volume, potentially improving sensitivity by incorporating the correlations among these neurodegeneration measures.

Because NfL is not specific to AD pathology, future predictive models should also integrate complementary biomarkers. Plasma p-tau217 could provide greater specificity for AD-related tau pathology,28 while plasma Aβ42/40 could characterize amyloid pathology and glial fibrillary acidic protein (GFAP) could reflect astrocytic activation.29 Combining these markers with NfL may help distinguish the presence of AD pathology from the intensity of ongoing neuroaxonal injury. Continuous amyloid and tau measures may also provide more information than binary Aβ classification. Additional factors such as APOE ε4 status, vascular disease burden, white-matter injury, baseline cognition, and baseline structural MRI abnormality could be evaluated where sample size permits. These approaches may ultimately provide more accurate individualized prediction than NfL alone.

In conclusion, this study established age-, BMI-, and eGFR-adjusted plasma NfL reference distributions and demonstrated that the resulting Z-scores captured group-level increases in neuroaxonal injury across the AD continuum. However, a single baseline NfL Z-score did not reliably predict subsequent hippocampal atrophy, AD-signature cortical

thinning, or ventricular enlargement in the available Aβ+ longitudinal cohorts. The preliminary association between longitudinal NfL increase and hippocampal volume decline raises the possibility that biomarker dynamics may provide information beyond a single measurement, although this finding requires confirmation in larger cohorts with more frequent repeated measurements. These results support the value of physiological adjustment for interpreting plasma NfL while indicating that individualized prediction of neurodegeneration will likely require longitudinal biomarker assessment, AD-specific biomarkers, and more comprehensive multimodal models.

References

1. GBD 2019 Dementia Forecasting Collaborators. Estimation of the global prevalence of dementia in 2019 and forecasted prevalence in 2050. *Lancet Public Health.* 2022;7: e105–e125.
2. Jia J, Ning Y, Chen M, et al. Biomarker changes during 20 years preceding Alzheimer's disease. *N Engl J Med.* 2024; 390:712–722.
3. Schaap T, Thropp P, Tosun D; for the Alzheimer's Disease Neuroimaging Initiative. Timing of Alzheimer's disease biomarker progressions: a two-decade observational study from ADNI. *Alzheimers Dement.* 2024; 20:9060–9067.
4. Rowley PA, Samsonov AA, Betthauser TJ, Pirasteh A, Johnson SC, Eisenmenger LB. Amyloid and Tau PET Imaging of Alzheimer Disease and Other Neurodegenerative Conditions. Seminars in Ultrasound, CT and MRI. 2020 Dec;41(6):572–83.
5. Jack CR Jr, Knopman DS, Jagust WJ, et al. Hypothetical model of dynamic biomarkers of the Alzheimer's pathological cascade. *Lancet Neurol.* 2010; 9:119–128.
6. Jack CR Jr, Wiste HJ, Weigand SD, et al. Defining imaging biomarker cut points for brain aging and Alzheimer's disease. *Alzheimers Dement.* 2017; 13:205–216.
7. Khalil M, Teunissen CE, Otto M, et al. Neurofilaments as biomarkers in neurological disorders. *Nat Rev Neurol.* 2018; 14:577–589.
8. Simrén J, Ashton NJ, Blennow K, Zetterberg H. An update on blood-based biomarkers for non-Alzheimer neurodegenerative disorders. *Nat Rev Neurol.* 2023; 19:358–377.
9. Rissin DM, Kan CW, Campbell TG, Howes SC, Fournier DR, Song L, et al. Single-molecule enzyme-linked immunosorbent assay detects serum proteins at subfemtomolar concentrations. Nature Biotechnology [Internet]. 2010 Jun 1;28(6):595–9. Available from: https://www.nature.com/articles/nbt.1641

10. Mattsson N, Zetterberg H, Janelidze S, et al. Plasma tau in Alzheimer disease. *Neurology.* 2016; 87:1827–1835.
11. Mattsson-Carlgren N, Andersson E, Janelidze S, et al. Aβ deposition is associated with increases in soluble and phosphorylated tau preceding a positive Tau PET in Alzheimer's disease. *Sci Adv.* 2020;6: eaaz2387.
12. Preische O, Schultz SA, Apel A, et al. Serum neurofilament dynamics predicts neurodegeneration and clinical progression in presymptomatic Alzheimer's disease. *Nat Med.* 2019; 25:277–283.
13. Pichet Binette A, Janelidze S, Cullen N, Dage JL, Bateman RJ, Zetterberg H, et al. Confounding factors of Alzheimer's disease plasma biomarkers and their impact on clinical performance. Alzheimer's & Dementia. 2022 Sep 24;
14. Benkert P, Meier S, Schaedelin S, et al. Serum neurofilament light chain for individual prognostication of disease activity in people with multiple sclerosis. *Lancet Neurol.* 2022; 21:246–257.
15. Zetterberg H, Blennow K. Moving fluid biomarkers for Alzheimer's disease from research tools to routine clinical diagnostics. *Mol Neurodegener.* 2021; 16:10.
16. Pomponio R, Erus G, Habes M, Doshi J, Srinivasan D, Mamourian E, et al. Harmonization of large MRI datasets for the analysis of brain imaging patterns throughout the lifespan. NeuroImage [Internet]. 2020 Mar 1; 208:116450. Available from: https://www.sciencedirect.com/science/article/pii/S1053811919310419
17. Singer W, Schmeichel AM, Sletten DM, Gehrking TL, Gehrking JA, Trejo-Lopez J, et al. Neurofilament light chain in spinal fluid and plasma in multiple system atrophy: a prospective, longitudinal biomarker study. Clinical Autonomic Research. 2023 Aug 21;33(6):635–45.
18. Jack CR, Arvin Arani, Borowski BJ, Cash DM, Crawford K, Das SR, et al. Overview of ADNI MRI. Alzheimer s & Dementia. 2024 Sep 11;

19. Dekkers IA, Jansen PR, Lamb HJ. Obesity, Brain Volume, and White Matter Microstructure at MRI: A Cross-sectional UK Biobank Study. Radiology. 2019 Jun;291(3):763–71.
20. Khalil M, Pirpamer L, Hofer E, Voortman MM, Barro C, Leppert D, et al. Serum neurofilament light levels in normal aging and their association with morphologic brain changes. Nature Communications [Internet]. 2020 Feb 10;11(1):812. Available from: https://www.nature.com/articles/s41467-020-14612-6
21. Syrjanen JA, Campbell MR, AlgecirasSchimnich A, Vemuri P, GraffRadford J, Machulda MM, et al. Associations of amyloid and neurodegeneration plasma biomarkers with comorbidities. Alzheimer's Dement [Internet]. 2022 [cited 2026 Jun 7];18(6):1128–40. Available from: https://doi.org/10.1002/alz.12466
22. Mattsson N, Cullen NC, Andreasson U, Zetterberg H, Blennow K. Association Between Longitudinal Plasma Neurofilament Light and Neurodegeneration in Patients with Alzheimer Disease. JAMA Neurology. 2019 Jul 1;76(7):791.
23. Arslan B, Zetterberg H, Ashton NJ. Integrating kidney function assessment into the clinical interpretation of plasma Alzheimer's disease biomarkers. Journal of Alzheimer's Disease [Internet]. 2025 Sep 9;108(1):75–8. Available from: https://pmc.ncbi.nlm.nih.gov/articles/PMC12541103/
24. Zheng HT, Wu Z, Mielke MM, Murray AM, Ryan J. Plasma Biomarkers of Alzheimer's Disease and Neurodegeneration According to Sociodemographic Characteristics and Chronic Health Conditions. The Journal of Prevention of Alzheimer's Disease [Internet]. 2024 Jul 14;11(5):1189–97. Available from: https://www.sciencedirect.com/science/article/pii/S2274580724006472
25. Kidney Disease: Improving Global Outcomes (KDIGO) CKD Work Group. KDIGO 2024 Clinical Practice Guideline for the Evaluation and Management of Chronic Kidney Disease. Kidney International [Internet]. 2024 Apr;105(4S): S117–S314. Available from: https://doi.org/10.1016/j.kint.2023.10.018

26. Stasinopoulos DM, Rigby RA. Generalized additive models for location scale and shape (GAMLSS) in R. Journal of Statistical Software [Internet]. 2007;23(7):1–46. Available from: https://doi.org/10.18637/jss.v023.i07
27. Jack CR Jr, Wiste HJ, Weigand SD, Therneau TM, Lowe VJ, Knopman DS, et al. Defining imaging biomarker cut points for brain aging and Alzheimer's disease. *Alzheimer's & Dementia*. 2017;13(3):205–216. https://doi.org/10.1016/j.jalz.2016.08.005
28. Palmqvist S, Janelidze S, Quiroz YT, et al. Discriminative accuracy of plasma phospho-tau217 for Alzheimer disease vs other neurodegenerative disorders. JAMA [Internet]. 2020 Aug 25;324(8):772–781. Available from: https://doi.org/10.1001/jama.2020.12134
29. Schindler SE, Bollinger JG, Ovod V, et al. High-precision plasma β-amyloid 42/40 predicts current and future brain amyloidosis. Neurology [Internet]. 2019 Oct 22;93(17):e1647–e1659. Available from: https://doi.org/10.1212/WNL.0000000000008081

Publishing Agreement

It is the policy of the University to encourage open access and broad distribution of all theses, dissertations, and manuscripts. The Graduate Division will facilitate the distribution of UCSF theses, dissertations, and manuscripts to the UCSF Library for open access and distribution. UCSF will make such theses, dissertations, and manuscripts accessible to the public and will take reasonable steps to preserve these works in perpetuity.

I hereby grant the non-exclusive, perpetual right to The Regents of the University of California to reproduce, publicly display, distribute, preserve, and publish copies of my thesis, dissertation, or manuscript in any form or media, now existing or later derived, including access online for teaching, research, and public service purposes.

Signed by:
Shuotong Liu
50A334D1778147A...
Author Signature

08/31/2026
Date